Bacillus subtilis-mediated weathering of basalt revealed through sporulation

Christopher Yip[1], *Kira Stonkevitch*[1,+], *Abigail Knecht*[1,+], *Philip D. Weyman*[1], *Tania Timmermann*[1], *Corey R. Lawrence*[1], *Gonzalo A. Fuenzalida-Meriz*[1,*]

[1]Andes Ag, Inc., Alameda, CA, USA

[*]Corresponding author: Gonzalo A. Fuenzalida-Meriz, gonzalofuenzalida@gmail.com

[+]KS and AK contributed equally to this manuscript

ABSTRACT

Silicate rock weathering is a naturally occurring process that provides a long-term sink for atmospheric CO_2, but its natural rates are too slow on human-relevant timescales to offset anthropogenic emissions. Microbial activity offers a potential mechanism for accelerating silicate mineral dissolution and subsequent CO_2 drawdown. Here, we investigated the role of *Bacillus subtilis* strains MP1 and MP2 in the weathering of basalt, a cation-bearing, silicate-rich rock. Incubation of basalt with MP1 or MP2 resulted in significantly increased levels of soluble calcium compared to uninoculated, abiotic controls. Using ICP-MS, we measured the release of other cations found in basalt, and we used a genetic strategy to demonstrate basalt-derived cation uptake during the sporulation process. Scanning electron microscopy revealed feldspar twinning features on basalt surfaces following microbial treatment, providing concrete evidence of silicate rock weathering; these micrographs also identified numerous ovoid cell structures, indicating the presence of bacterial spores at the mineral surface. Because sporulation is known to require cations including Ca^{2+}, Mg^{2+}, and Mn^{2+}, these findings together establish MP1 and MP2 as active agents of basalt weathering and highlight *Bacillus* sporulation as a potential bio-indicator for silicate dissolution. By linking microbial physiology with geochemical processes, our results highlight how strain-specific interactions with rock compositions could inform silicate weathering strategies for carbon dioxide removal, including enhanced weathering and microbially-accelerated weathering.

KEYWORDS

Bacillus subtilis strain MP1, *Bacillus subtilis* strain MP2, sporulation, scanning electron microscopy (SEM), microbially-accelerated weathering, carbon dioxide removal (CDR).

INTRODUCTION

Silicate weathering is a fundamental geochemical process that regulates Earth's carbon cycle and has been central in stabilizing the global climate over millennia by generating a sink for carbon dioxide (CO_2)[1–3]. In the weathering process and at the most basic level, silicate minerals found ubiquitously throughout terrestrial environments react with a variety of acids, including organic acids from microbial and plant origin, and carbonic acid formed from atmospheric CO_2 and water[4,5]. Weathering liberates soluble metal cations from native silicates, and alkalinity is generated as a result of this process[3–5]. The resulting alkalinity is enriched for soluble bicarbonates and carbonates, and is transported through the soil column, eventually reaching the oceans, where it is estimated to be stable for thousands of years[6,7]. As such, silicate weathering ultimately captures and removes atmospheric CO_2 and stores the carbon as stable carbonates and bicarbonates across geological timescales.

Because rates of silicate weathering are too slow to meaningfully counteract anthropogenic CO_2 emissions on timescales relevant to climate mitigation, new applications, practices, and technologies that facilitate more rapid silicate weathering are urgently needed, in combination with reducing CO_2 emissions themselves. In recent years, enhanced weathering (EW) has emerged as a promising strategy for CO_2 removal by applying silicate minerals to soils[8–12]. Supplementation of soils with crushed silicate minerals can mitigate soil acidification, and the increased mineral surface area accelerates silicate weathering and subsequent carbon dioxide removal (CDR). Among the potential EW feedstocks, basaltic rocks are of particular interest. Basalt is one of the most abundant volcanic rocks on Earth and is rich in silicate minerals such as olivine, pyroxene, and plagioclase[13]. The widespread availability of basalt and its capacity to release divalent cations

(e.g., Ca^{2+} and Mg^{2+}) make it an attractive candidate for large-scale deployment in agricultural settings for CDR efforts[14]. In addition to their ability to charge balance and stabilize bicarbonate ions, the cations released by weathering have many co-benefits, including improving soil pH, soil fertility, and plant health[15,16].

An alternative strategy to EW is the addition of specific microorganisms to soils that are already rich in cation-bearing silicate minerals[17]. This strategy, termed microbially-accelerated weathering (MAW, formerly microbial carbon dioxide mineralization (MCM)), leverages naturally-occurring microbes, specifically their cellular processes and metabolisms, to accelerate the dissolution of native silicates without requiring additional rock applications. Microorganisms, particularly bacteria and fungi, are increasingly being recognized as active participants in silicate weathering[17–22]. Microbes and microbial communities can increase silicate dissolution rates relative to abiotic processes by altering the local pH and redox conditions[17,23]. These microbes and microbial communities can also produce and secrete diverse panels of biomolecules such as organic acids, chelators, enzymes, and various other redox-active metabolites[19,21,22,24–26]. Among the microbes that promote weathering, *Bacillus* species have attracted considerable attention for their ability to colonize mineral surfaces and mobilize silicate-bound nutrients[27]. *B. mucilaginosus* and *B. edaphicus* are known to produce low molecular weight organic acids (e.g., oxalic and citric acids) that solubilize potassium and silicon from aluminosilicate-minerals, providing plant nutrients and improving soil fertility[25,28,29].

Despite the growing evidence of microbial contributions to silicate rock weathering, far less is currently understood about how these interactions can subsequently affect microbial

physiology[19,26]. Many cellular processes are influenced by metal availability, including sporulation, and the ways microbes influence and respond to silicate weathering remain largely unexplored. Understanding physiological responses may reveal biological indicators for tracking microbially-accelerated silicate weathering and could couple biochemical processes to CDR strategies.

We previously reported that *B. subtilis* strain MP1 (herein referred to as "MP1") accelerated the weathering of anorthite, a calcium rich feldspar, and promoted the formation of soil inorganic carbon under both laboratory and field conditions[17]. A recent soil mesocosm study demonstrated that MP1 also improved the weathering of basalt, resulting in a significant increase in soil alkalinity[18]. These findings established MP1 as an effective biological agent of silicate weathering and provided foundational evidence that microbial activity can drive silicate mineral dissolution and subsequent carbon dioxide removal in agricultural soils. MP1, however, is not genetically tractable, limiting genetic approaches to understanding the biochemical mechanisms of action of microbial-mediated silicate weathering. To overcome this limitation, we employed *Bacillus subtilis* strain MP2 (herein referred to as "MP2"). MP2 shares approximately 99% DNA nucleotide sequence identity with MP1, but can be readily modified using standard genetic tools. The close genetic relatedness between MP1 and MP2 enables direct comparison of their weathering capabilities while facilitating the generation of defined mutants to interrogate weathering-associated cellular processes. Accordingly, MP2 serves as a genetically tractable surrogate for MP1, enabling mechanistic analyses of *Bacillus*-mediated silicate weathering.

In line with our previous findings, when calcium release was measured as a proxy for silicate weathering under *in vitro* conditions, we consistently observed a decrease in soluble calcium at later timepoints[17]. We speculated that the decrease in calcium levels could be due to the onset of sporulation, a cellular process requiring uptake of calcium, and/or the precipitation of insoluble carbonates or other secondary mineral phases as the pH gradually becomes more alkaline. Consistent with this, high spore titers were recovered from our established *in vitro* weathering assays and scanning electron microscopy revealed basalt surfaces were heavily populated with *Bacillus* spores. Given that spore formation in *B. subtilis* requires metals such as Ca^{2+}, $Fe^{2+/3+}$, and Mn^{2+}, which are also found abundantly in rocks such as basalt, we hypothesized that sporulation could serve as a biological indicator of microbially-accelerated silicate weathering[30]. Our findings support this hypothesis and provide new insight into the physiological responses of *B. subtilis* during silicate weathering. Furthermore, the microbe's ability to procure the metals needed for sporulation from the rock is evidence of its ability to promote and accelerate rock weathering. By linking microbial metabolism and physiology to basalt weathering dynamics, our findings expand the understanding of microbial contributions to enhanced weathering and offer a framework for developing biologically informed CDR strategies.

RESULTS

Bacillus subtilis accelerates the weathering of basalt.

To determine the extent to which *Bacillus subtilis* strains MP1 and MP2 accelerate silicate weathering and mobilize cations, the microbes were cultured in liquid mB4-1 medium with and without basalt over a seven day time course (Figure 1 and Supplemental Figure S1). At each timepoint, the cultures were harvested and the supernatants were analyzed for soluble calcium

derived from basalt-associated mineral dissolution. In the uninoculated control (UTC) containing basalt, calcium concentrations gradually increased to approximately 0.44 mM by day 7 (Figure 1A, solid orange line). In contrast, MP1 and MP2 cultures released significantly ($p < 0.0001$) higher calcium in the presence of basalt, reaching approximately 1.8 mM and 1.1 mM on day 7, respectively (Figure 1A, solid gray and green lines). In samples lacking basalt, calcium measurements remained low, demonstrating that the calcium increases are derived only from the basalt substrate (Figure 1A, dashed lines). The elevated calcium observed with the samples containing both microbes and basalt suggests the liberated calcium was likely a consequence of microbially-accelerated weathering of basalt.

To corroborate our in-house calcium measurements, ICP-MS was also performed on a subset of culture supernatants. ICP-MS measurements for calcium showed the same overall trend across three timepoints, comparing UTC and MP2 in the presence and absence of basalt (Figure 1A and Supplemental Figure S2). In the absence of microbial inoculum (UTC), calcium levels gradually increased (0.42 → 0.61 → 0.81 mM) across the three timepoints in the presence of basalt. In-house measurements of MP2 supernatants on days 2 and 7 showed ~1.4 mM and ~1.0 mM calcium, respectively, whereas ICP-MS of the same samples measured ~1.7 mM and ~1.5 mM, respectively. These results support the observation that the increase in soluble calcium resulted from basalt dissolution that was accelerated by microbial treatment, rather than an artifact of our in-house quantification assay.

Compared to MP1 cultures grown with calcium-bearing feldspars, MP2 exhibited strikingly similar pH dynamics when cultured with basalt (Timmermann et al., 2025, and Figure 1B). In the

absence of basalt, MP2 initially decreased the media pH by day 1, then gradually raised the alkalinity to pH 7 by the end of the experimental time course (Figure 1B, dashed green line). MP2 co-cultured with basalt exhibited a more subtle, and smaller decrease in pH than without basalt by day 1 but then caused a rapid increase in pH, which was eventually stabilized near pH 9 (Figure 1B, solid green lines). Additionally, in the presence of basalt, MP1, MP2, and Δ*spoIIE* exhibited robust pellicle formation; pellicle formation and mature biofilms were absent from samples containing mB4-1 media alone (Supplemental Figure S1).

Bacillus subtilis **MP1 and MP2 can undergo sporulation in the presence of basalt.** We have consistently observed a decrease in soluble calcium with MP1 and MP2 after day 2 of our *in vitro* weathering experiments with both feldspar and basalt (Timmermann et al., 2025, and Figure 1A, respectively). We hypothesized that this decrease could be partially attributed to the onset of sporulation and the formation of mature spores, which are known to take up calcium from the medium[31–33]. To test this hypothesis, we quantified the total number of cells and spores from cultures grown in the presence and absence of basalt after three days of incubation (Figure 2). Approximately 10^7 CFU/ml total viable cells were recovered from MP1 and MP2 cultures grown without basalt. Under basalt-free conditions, spore-forming units were recovered at approximately 10^3 spores/ml for MP1 and 10^4 spores/ml for MP2. In contrast, in the treatments where basalt was added, the total viable cell counts remained similar; however, spore counts increased substantially by ~4-log and ~2.5-log for MP1 and MP2, respectively (Figure 2). This large increase in the number of spores and sporulation efficiency suggests that the microbes can weather basalt rocks, which then releases metals required for the induction of sporulation (e.g., Ca^{2+}, Mg^{2+}, K^{+}, Mn^{2+}, and $Fe^{2+/3+}$).

To determine whether the decrease in calcium was directly linked to the onset of sporulation and mature spore formation, we generated and examined a Δ*spoIIE* sporulation-deficient strain of MP2. The Δ*spoIIE* strain was unable to produce spores when cultured under standard sporulation promoting conditions (Supplemental Figure S3). When tested in an *in vitro* basalt weathering assay, Δ*spoIIE* exhibited robust vegetative growth, and the total viable cell counts from the mutant strain were similar to MP1 and MP2 in both the presence and absence of basalt (Figure 2, purple bars). As expected, the Δ*spoIIE* strain was unable to produce spores in either the presence or absence of basalt. When Δ*spoIIE* was cultured in the presence of basalt, calcium levels remained elevated well beyond day 2, a point at which MP1 and MP2 calcium levels began to decline (Figure 1A, solid blue line). After day 5, the calcium levels following Δ*spoIIE* treatment remained elevated and had plateaued up until the final timepoint of our experiment. At the day 7 timepoint, calcium levels remained significantly elevated with Δ*spoIIE* in comparison to MP1 ($p < 0.01$), and its wild type counterpart MP2 ($p < 0.0001$) (Figure 1A). Indeed, ICP-MS analysis of calcium from Δ*spoIIE* supernatants confirmed the same phenomena (Supplemental Figure S2). The calcium data support our hypothesis that sporulation is significantly induced by the products of weathering basalt and that sporulation is partially responsible for the decline in calcium during the course of basalt weathering under our laboratory conditions.

Since basalt is composed of various metal-bearing silicates, we also questioned whether a similar decline could be observed with other metals. Manganese is an essential metal required for the induction of sporulation and the formation of mature spores[34,35]. ICP-MS of uninoculated media containing basalt revealed relatively low concentrations of manganese that slowly increased over

time (0.23 → 0.90 → 1.45 μM at days 0, 2, and 7), likely due to abiotic weathering (Supplemental Figure S2). In contrast, the concentration of soluble manganese rose sharply in the presence of MP2 by day 2, then declined by day 7 (0.28 → 4.10 → 0.70 μM). The initial increase in manganese points to MP2's ability to accelerate basalt weathering, while the subsequent decrease is in line with MP2's ability to take up manganese during the process of sporulation (Figure 2). This pattern, however, was not observed with Δ*spoIIE*, which instead showed a gradual increase in manganese across the three timepoints tested (0.27 → 2.57 → 4.24 μM). The elevated levels of manganese on day 7 are in line with Δ*spoIIE*'s inability to undergo sporulation, and reveals a more accurate measurement of the release of this element from basalt in the absence of sporulation as a sink.

Magnesium, another element known to be important for sporulation, also had lower concentrations on days 2 and 7 in MP2 relative to Δ*spoIIE* (Supplemental Figure S2). Additionally, silicon levels increased sharply for Δ*spoIIE* relative to UTC, suggesting the microbes are accelerating the dissolution of silicates. Interestingly, while the *spoIIE* mutation should not affect the strain's ability to accelerate the weathering of silicate minerals, silicon levels remained low for MP2 which could be attributed to MP2 taking up dissolved silicon from the medium during sporulation[36].

Mineral substrates lacking key metals cannot induce *Bacillus* sporulation. Difco Sporulation Medium (DSM), a standardized medium for producing *B. subtilis* endospores, contains several cations, notably Ca^{2+}, $Fe^{2+/3+}$, K^{+}, Mg^{2+}, and Mn^{2+}, that can induce spore formation and allow for the formation of mature spores (Supplemental Figure S3)[30,34,35,37,38]. To test whether the presence of specific metals influences sporulation, MP2 cultures were incubated for three days in mB4-1 medium with or without different mineral substrates (Figure 3). Importantly, mB4-1

alone cannot efficiently trigger *Bacillus* sporulation due to the absence of essential metals (Figures 2 and 3). Given the heterogeneous mixture of silicates and silicate-bound metals found in basaltic rocks, we hypothesized that the weathering of basalt releases essential metals, such as Mn^{2+}, that can trigger sporulation. Alternatively, substrates that lack this panel of essential metals should not significantly trigger sporulation or affect the sporulation efficiency.

MP2 cultures grown in the presence and absence of metal-bearing substrates exhibited similar total viable cell counts (~10^7 CFU/ml, Figure 3). In the absence of substrate, we recovered approximately 10^5 spores/ml from MP2 (sporulation efficiency <1%). Consistent with our hypothesis, MP2 grown in the presence of basalt exhibited an approximate 2-log increase in the number of spores, relative to the no-substrate control; this increase in spore count corresponded to a sporulation efficiency of approximately 56%. In contrast, when MP2 was co-cultured with dolomite, a calcium-magnesium rich carbonate mineral that lacks other metal cations required for sporulation, minimal spore formation (sporulation efficiency <1%) was observed while total viable cell counts were comparable to the no-substrate control and basalt sample. Consistent with our strains' ability to weather minerals, MP1, MP2, and Δ*spoIIE* could also liberate calcium from dolomite (Supplemental Figure S4). These findings demonstrate that sporulation of *Bacillus* strains cannot be induced solely by the presence of calcium or magnesium (as in the case with dolomite), but instead relies on accessing a broader suite of trace metals released from silicate substrates such as basalt.

Basalt weathering by MP2 and Δ*spoIIE* releases soluble cations that induce sporulation.

We next questioned whether *B. subtilis* co-cultured with basalt could reconstitute a spore-inducing medium from a medium that normally cannot trigger *Bacillus* sporulation. We hypothesized that MP2 and Δ*spoIIE* can weather basalt to release metals from silicate minerals that another cultured microbe could then use to grow and trigger sporulation. To determine if the interaction between *B. subtilis* and basalt could generate weathering products (i.e., Ca^{2+}, $Fe^{2+/3+}$, K^{+}, Mg^{2+}, and Mn^{2+}) capable of triggering sporulation in other cells, we assessed cell-free, "spent" supernatants generated from UTC or Δ*spoIIE* grown in the presence and absence of basalt for 3 days.

MP2 and Δ*spoIIE* grew to similar cell densities (~10^7 CFU/ml) when cultured in fresh nutrient broth, spent nutrient broth lacking basalt, and Δ*spoIIE*-spent nutrient broth containing basalt indicating that growth was not limited by nutrient depletion in either of the microbially spent media (Figure 4, purple). In fresh nutrient broth (NB) and Δ*spoIIE*-spent nutrient broth lacking basalt (-BA Spent NB), MP2 exhibited minimal sporulation (approximately 10^2-10^3 spores/ml). Strikingly, MP2 grown in spent nutrient broth derived from Δ*spoIIE* cultured in the presence of basalt (+BA Spent NB) showed a drastic and significant ($p < 0.01$) increase in spore CFUs (Figure 4). This increase in spore counts corresponded to a sporulation efficiency of approximately 74% compared to 28% with UTC-spent nutrient broth (Supplemental Table S4). As expected, we were unable to recover or detect any Δ*spoIIE* spores under any of the conditions tested. Together, these findings suggest that Δ*spoIIE* and MP2 can weather silicates to release soluble metal ions into the surrounding medium, and these metals can induce sporulation in *B. subtilis* (Figures 2, 3, and 4).

Basalt surfaces incubated with MP1 and MP2 reveal feldspar twinning and are heavily populated with *Bacillus* spores.

After demonstrating the positive effects of MP1 and MP2 on basalt dissolution by measuring calcium, accumulation of other metals, and sporulation efficiencies, we next examined whether the apparent weathering activity could manifest observable changes to basalt surfaces. We conducted scanning electron microscopy (SEM) analyses on polished basalt surfaces in the presence and absence of microbial colonization. In the absence of microbes, the UTC exhibited no microbial colonization (Figure 5 and Supplemental Figure S5). In contrast, basalt incubated with MP1 and MP2 were heavily colonized (Figure 5 and Supplemental Figure S5). Upon closer examination of the cell morphologies at higher magnifications (2000x and 4000x), the basalt rocks were heavily populated with ovoid structures approximately 1 μm in length (Figure 5). The size and shape of these structures are consistent with *Bacillus subtilis* spores. In line with our datasets, approximately 10^7 spores/ml were recovered from MP1 and MP2 after the 30-day incubation (Supplemental Table S5).

Interestingly, colonization of the rock surfaces was not apparent/observed when the basalt was incubated with Δ*spoIIE* (Figure 5, '*ΔspoIIE'*). Although Δ*spoIIE* cells were not detected on basalt surfaces, viable cell counts were recovered after the 30-day incubation period, but no viable spores could be recovered, as expected (Supplemental Table S5). This absence likely reflects that the drying and downstream SEM sample preparation processes are too harsh for vegetative cells to survive. Another possibility is that *Bacillus* spores have additional adhesion factors that allow them to attach to and retain onto the basalt disks, whereas vegetative cells cannot.

Evidence of silicate weathering can often manifest as micropitting or etching on mineral surfaces[39–41]. As expected, we were unable to find evidence of weathering in our UTC sample, as

pitting and etching were visually absent, and the mineral surfaces remained smooth. In contrast, we observed structured, striation-like features on the surfaces of the basalt disks incubated with MP1, MP2, and Δ*spoIIE* (Figure 5, red arrows). These features are likely twinning of feldspar minerals within the basalt rock, a phenomenon related to geometric crystalline growth[42]. The presence and greater abundance of these features relative to the UTC sample suggests enhanced mineral dissolution driven by the microbes. We observe these phenomena for Δ*spoIIE* despite not detecting cells in the micrographs, consistent with the idea that these features are the result of weathering during the 30 day incubation, and the lack of visible cells for Δ*spoIIE* reflects the harsh SEM sample preparation conditions that may not allow vegetative cells to persist.

DISCUSSION

The positive effects of MP1 on feldspar weathering prompted us to evaluate whether a similar phenomenon would occur with basaltic rocks[17]. Importantly, the relatively high abundance in native soils, widespread availability in quarries, and the capacity of basalt to release divalent cations relevant to carbon dioxide removal make it an attractive candidate for MAW and EW practices. To examine the effect of *B. subtilis* environmental isolates MP1 and MP2 on basalt weathering, we utilized a similar weathering screen as previously described[17]. In uninoculated controls containing basalt, elemental concentrations of calcium, iron, lithium, magnesium, manganese, and silicon all gradually increased, which we attributed to abiotic dissolution and the release of readily accessible surface ions (Figure 1A and Supplemental Figure S2). In contrast, MP1 and MP2, when co-cultured with basalt, solubilized four- to six-fold more calcium on day 2 relative to the uninoculated controls when measured by our in-house quantification assay (Figure

1A). Similarly, MP2 and Δ*spoIIE* solubilized two- to four-fold more calcium relative to UTC when the same samples were measured by ICP-MS (Supplemental Figure S2).

Silicate weathering is widely recognized as a pH-dependent process[4,43,44]. Across all conditions tested, MP1, MP2, and Δ*spoIIE* initially decreased the media pH by day 1, independent of substrate type or substrate addition. However, in the presence of basalt, the cultures exhibited a smaller decrease in pH, relative to cultures lacking substrate, which could be attributed to basalt acting as a sink for H^+ (Figure 1B). Silicate weathering, which consumes protons and thus raises pH, leads to the release of base cations and alkalinity. As previously observed during feldspar weathering, we propose that these pH dynamics are also exaggerated and driven by microbial metabolism in response to cation-bearing silicate substrates and serve to promote mineral dissolution[17]. Accordingly, MP1, MP2, and Δ*spoIIE* accelerated and enhanced the dissolution of basalt which resulted in the release of soluble aluminum, calcium, iron, magnesium, manganese, and silicon above abiotic levels, which is consistent with microbially-accelerated weathering (Figure 1A and Supplemental Figure S2).

The concentration of certain soluble metals and base cations is expected to increase over time and remain elevated during silicate dissolution. However, we consistently observed a decline in soluble calcium after day 2 with both anorthite and basalt during our *in vitro* weathering assays[17]. Notably, cation decline has also been observed in closed system experiments, raising the possibility that our observations could reflect general geochemical behaviors of basalt weathering in closed systems rather than biologically driven processes[45–47]. In abiotic, poor drainage systems, basalt glass dissolution has been shown to form secondary minerals with soluble magnesium precipitating into

328 brucite within ~20 hours; as the system increased in alkalinity beyond 54 hours, smectite, a
329 calcium-magnesium rich clay formed and became the dominant cation sink[48,49]. Thus, we
330 considered whether secondary mineral/clay formation could explain our observed decline. In our
331 inoculated cultures, the pHs also rose to comparable alkaline levels at later timepoints so we cannot
332 fully exclude the contribution of secondary mineral formation to the observed calcium decline
333 (Figure 1B). However, while MP1, MP2, and Δ*spoIIE* exhibited similar pH dynamics in the
334 presence of basalt, the elevated levels of calcium in Δ*spoIIE* argue against abiotic precipitation as
335 the dominant driver observed with MP1 and MP2, since a purely geochemical mechanism would
336 be expected to affect all three strains similarly[46,47].
337
338 To assess the favorability of secondary mineral formation, we calculated the approximate mass of
339 basalt that would be required to drive the maximum calcium concentrations as measured by ICP-
340 MS from UTC (day 2) and Δ*spoIIE* (day 7) samples containing basalt. Using the measured weight
341 fraction of calcium in the BrixBlend basalt (0.067 g Ca per g basalt), approximately 1.2 mg basalt
342 and 2.8 mg basalt would need to be weathered in the UTC and Δ*spoIIE* treatments, respectively,
343 representing 2.4% and 5.6% of the added basalt (Supplemental Table S3). Using these estimates
344 of basalt dissolution and the measured basalt chemistry, the maximum concentrations of other
345 major elements in solution were also estimated assuming stoichiometric basalt weathering. This
346 assumption, however, is unlikely to be true because the various mineral phases within basalt are
347 known to weather at different rates, but this nonetheless provides a useful starting point in the
348 absence of mineral specific data.
349

The estimated maximum concentrations for several major elements contributing to secondary phase formation (Al, Si, Mg, and Fe) were higher than the corresponding measured maximum concentrations, suggesting secondary mineral formation could be removing weathering products from solution. To support this interpretation, we initialized a simple geochemical speciation model (CrunchFlow, speciate-only) using the estimated maximum concentrations and measured pH values to calculate the saturation indices for a range of possible secondary mineral phases (Supplemental Figure S6). The results suggested that both UTC and Δ*spoIIE* treatments would be oversaturated with respect to several common secondary phases including kaolinite, gibbsite, goethite, and smectite (i.e., Ca bearing montmorillonite) at the time of peak calcium concentrations. However, only Δ*spoIIE* was overmatured with respect to calcite. These results further support the interpretation that secondary mineral formation, in addition to sporulation, is removing some weathering products from solution. However, given that calcium concentrations rise to a greater extent between days 2 and 7 in Δ*spoIIE* compared to UTC, it is likely that biological weathering continues to dissolve basalt as secondary phases accumulate. In contrast, the lower rate of calcium release between day 2 and 7 of the UTC treatment suggests abiotic mineral dissolution has slowed in that treatment.

Our hypothesis of microbially-accelerated silicate weathering was supported by the measured release of soluble aluminum, calcium, iron, magnesium, manganese, and silicon above abiotic levels. Surprisingly, when lithium was measured from culture supernatants, the concentrations gradually increased over time across all three treatment groups (UTC, MP2, and Δ*spoIIE*), reaching similar levels by day 7 (1.33, 1.17, and 1.49 μM, respectively; Supplemental Figure S2). While lithium is commonly used as a tracer of basalt weathering, it is preferentially included in

373 secondary clay mineral formation, especially at alkaline pHs. Given the observed differences in
374 other elements that are characteristic of silicate weathering, we take this as evidence of secondary
375 clay formation in the basalt amended treatments.
376
377 We speculate that there are at least two potential mechanisms for the observed decline in free
378 cations/calcium following weathering: the precipitation of carbonate or other Ca bearing secondary
379 minerals, and the uptake of calcium through cellular processes (sporulation and biofilm formation).
380 When the highest levels of calcium were measured on day 2 for MP2, the pH of the cultures
381 containing basalt was below 8, making substantial $CaCO_3$ precipitation unlikely at this timepoint
382 (Figure 1). Below pH 8, the total inorganic carbon species exist predominantly as bicarbonate,
383 with only a very small fraction existing as carbonic acid and carbonate. The more pronounced
384 decline in calcium was not observed until day 5 of the *in vitro* weathering assay, which coincided
385 with a further rise in pH toward ~8.3, where the pH is expected to shift a larger proportion of
386 calcium bicarbonate to insoluble calcium carbonate.
387
388 Sporulation in *Bacillus* species is known to require substantial amounts of calcium. In the presence
389 of basalt, MP1 and MP2 exhibited significantly higher spore counts despite having similar total
390 viable cell counts relative to the no-substrate controls (Figures 2 and 3). In contrast, the Δ*spoIIE*-
391 derivative of MP2 maintained comparable vegetative cell growth in the presence of basalt but was
392 unable to form heat-resistant spores and did not exhibit a decrease in calcium (Figures 1A and 2,
393 and Supplemental Figure S2). These observations indicated that sporulation contributed to soluble
394 calcium depletion during basalt weathering, although it is unlikely to be the sole sink for the
395 released calcium. Indeed, while calcium was incorporated into spores, a substantial fraction of the

total calcium released from the weathering of basalt remains available for downstream geochemical processes, including the formation of secondary phases, bicarbonates, and carbonates relevant to CDR strategies.

ICP-MS data suggests manganese and silicon exhibited trends that were similarly influenced by microbial metabolism and physiology under our experimental conditions. In UTC samples, both manganese (0.23 → 0.90 → 1.45 μM) and silicon (0.04 → 0.04 → 0.08 mM) increased over time (Supplemental Figure S2). Δ*spoIIE* released substantially more manganese (0.27 → 2.57 → 4.24 μM) and silicon (0.04 → 0.08 → 0.21 mM) relative to the UTC controls. In the presence of MP2, the concentration of manganese initially increased from day 0 to day 2 (0.28 → 4.10 μM), but then dropped to 0.70 μM by day 7; this observed decline is likely due to uptake during the production of mature spores, precipitation of carbonate minerals, and formation of secondary phases at alkaline pHs, similar to calcium. Interestingly, silicon release was not apparent when MP2 was co-cultured with basalt. Unlike the steady increases observed with UTC and Δ*spoIIE*, soluble silicon in MP2 cultures remained low and largely unchanged across the three timepoints tested. We hypothesize that MP2 may incorporate solubilized silicon into the spore coats during sporulation, a process that has been reported with some *Bacillus* species[36].

Having identified sporulation as a relevant sink for calcium and other metals during basalt weathering, we investigated whether sporulation could serve as a physiological indicator for silicate weathering in a defined medium. Measurements of released calcium provide useful geochemical evidence for weathering activity but have some limitations. First, measurements of released metals do not provide insight into the physiological responses of microbial cells to

weathered products. Second, these measurements cannot discriminate between weathering of complex silicate mineral-containing rocks that release a variety of metals versus weathering of non-silicate minerals that may release only a small subset of the metals required for sporulation (e.g., calcium magnesium carbonates). Using alternative mineral substrates, we demonstrated that although MP1 and MP2 were capable of liberating calcium from dolomite, sporulation was not induced, indicating that calcium and magnesium alone are insufficient to trigger this developmental response (Figure 4). Furthermore, cell-free spent media generated from Δ*spoIIE* cultures incubated with basalt strongly induced MP2 sporulation, whereas spent media derived from Δ*spoIIE* grown without basalt had no such effect (Figure 4 and Supplemental Table S4). These findings confirm that Δ*spoIIE* was able to weather basalt and extract key elements such as Mn^{2+} and $Fe^{2+/3+}$ for the induction of sporulation, and Ca^{2+} for the formation of mature spores in *B. subtilis*. Our findings suggest soluble products of basalt weathering can trigger sporulation and that sporulation may serve as a complementary indicator for silicate weathering by *Bacillus*.

The calcium measurements and presence of microbial spores under basalt treatment provided complementary geochemical and physiological evidence for microbial-mediated weathering of basalt. We therefore investigated whether this activity could also be accompanied by detectable physical changes to basalt surfaces. Twinning is a characteristic crystalline structure that can commonly occur in feldspar minerals and is formed from the intergrowth of two or more crystal lattices[50,51]. As these crystalline structures exist naturally within feldspars, we hypothesized that the dissolution of silicate minerals through weathering processes could expose underlying twinning structures. SEM analyses of basalt disks treated with MP1, MP2, and Δ*spoIIE* revealed prominent striation-like features that are consistent with feldspar twinning. Importantly, these

features were conspicuously absent from uninoculated controls. We propose that while the twinning features are likely present in all of the original silicate rock samples, the increased visibility of these features in the presence of microbes is consistent with microbially-accelerated weathering of basalt.

Collectively, these findings establish *Bacillus subtilis* MP1 and MP2 as active and effective biological agents capable of enhancing basalt weathering under controlled *in vitro* conditions. Beyond increased cation release, this work identifies sporulation as a sensitive physiological indicator for microbial access to mineral-derived metals and extends prior observations of microbially-accelerated feldspar weathering to compositionally-complex and environmentally-relevant basalt rocks. The ability of *Bacillus* species to integrate mineral dissolution products into developmental processes highlights a tight coupling between microbial physiology and environmental geochemistry.

Future work should focus on identifying specific chemical species, biomolecules, and molecular mechanisms that mediate basalt dissolution by *Bacillus*. This information will be critical for understanding how these processes operate in soils and other natural environments. Determining how microbial physiology, mineral composition, and environmental conditions interact to regulate weathering rates will help guide biologically informed strategies for enhancing silicate weathering. Ultimately, integrating microbial processes into enhanced weathering frameworks (e.g., Yang et al., 2026) may provide a scalable and mechanistically grounded approach for accelerating carbon dioxide removal through microbially-accelerated silicate dissolution.

MATERIALS AND METHODS

Isolation and identification of strain MP2.

Bacillus subtilis strain MP2 is a naturally occurring soil microbe isolated from bunchgrass roots and rhizosphere soil samples from Imperial County, California, USA. Root samples with rhizosphere soil attached were collected and stored in a clean plastic bag. Soil and roots were divided into two samples (roots and rhizosphere soil), and portions of each sample were plated on LB-Lennox agar medium (1% tryptone, 0.5% yeast extract, 0.5% NaCl, 1.5% agar). MP2 was recovered as colonies from both rhizosphere soil and root samples.

Genome sequencing of MP2 was performed by Macrogen, Inc. (South Korea) using both PacBio and Illumina reads, and the resulting assembled genome was annotated with Bakta[52]. MP1 and MP2 genomes were aligned with Mauve embedded in the Geneious Prime software package (version 2025.1.2) and were found to have a pairwise identity of 99.1%. MP1 and MP2 each share 86% pairwise identity with the common reference strain *Bacillus subtilis* subsp. *subtilis* strain 168.

Generation of Δ*spoIIE* mutant.

A deletion of the open reading frame (ORF) encoded by gene *spoIIE* was generated using homologous recombination in strain MP2. First, a plasmid was constructed using Gibson Assembly that consisted of 1) a 985-bp left homology region upstream of the *spoIIE* ORF that ended 15-bp before the start codon, 2) a 1230-bp spectinomycin cassette that was ordered as a gBlock, 3) a 930-bp right homology region downstream of the *spoIIE* ORF and including the last 5-bp of the *spoIIE* ORF sequence, and 4) the vector pBR322 replacing the tetracycline resistance gene. Each fragment had sequence overlaps of 25-bp to adjacent fragments. Primers for the left

homology region were 5'-TCCTAATGCATGTCTTCCGAGCTGGCAAGTAGCCTTGTTGACAC and 5'-ATATGTAAGATTTAAATGCAACCGCCTGTTATATTCGTTGCCTGT. Primers for the right homology region were 5'-AATAGGGGGATCTTCTCGAGATAACATAACGCTTCCGTATAAATCA and 5'-TGCTCACGTCAGTCCCATCGACGTTTCTGCCAAATACACAATTCC. The assembled plasmid was sequenced and transformed into MP2 using natural transformation protocols and selection with spectinomycin[53]. Correct insertion was confirmed by PCR amplification of the entire left homology-spectinomycin resistance-right homology region from primers outside the homology arms and sequencing using Nanopore. The sporulation deficient phenotype was verified by the lack of spores after culturing in Difco Sporulation Medium.

Silicate rock and mineral preparation for weathering assays.

Commercially available basalt (BrixBlend, from Pioneer Valley, MA, Fedcoseeds.com) was sieved to <710 μm particles using a no. 25 test sieve (VWR# 57334-268). Detailed mineral and elemental compositions can be found in Supplemental Tables S1 and S2. To remove available cations and easily weatherable carbonates, 60 g sieved basalt was resuspended in 600 ml 1 mM HCl and incubated at room temperature for 5 minutes. The basalt was then pelleted at 2000 x g for 5 minutes and the supernatant was decanted and discarded. The basalt pellet was washed an additional time with HCl, followed by two additional washes with distilled water. The basalt was dried overnight at 60 °C, then sieved an additional time through a no. 25 test sieve. Dolomite was purchased as white quartz powder (Sigma-Aldrich) and was later found to be dolomite by XRD analysis.

Strain growth conditions, *in vitro* weathering assay, and analysis.

B. subtilis strain MP1 and *B. subtilis* MP2-derived strains were routinely cultured at 30 °C in LB-Lennox medium. Basalt *in vitro* weathering assays were conducted over 3- and 7-day time courses and performed as follows: Exponential phase cultures were diluted into mB4-1 (0.2% yeast extract, 0.3% casamino acids, 0.5% glucose, pH 7.3) to a final OD_{600} of 0.1. Two milliliters of the diluted cultures was transferred to 24-well plates with or without 50 mg acid-washed basalt or other substrates, with three independent biological replicates established for each strain, substrate condition, and timepoint. The plates were sealed with breathable membranes and incubated without shaking at 30 °C. At specified timepoints, the biofilms were disrupted, and the cultures were homogenized by repeated pipetting. Approximately 1.5 ml of the cultures were collected, pelleted, and 1 ml of the clarified supernatants was assayed for pH and soluble calcium. To measure pH, 199 µl of clarified supernatants was added to a 96-well plate, then mixed with 1 µl 0.5% phenol red for a final concentration of 0.0025% phenol red. The sample absorbances were measured at 570 nm, then fitted against a 12-point sigmoidal curve with standards ranging from pH 5 to pH 9. Soluble calcium, liberated as a byproduct of basalt weathering, was measured using the QuantiChrom™ Calcium Assay Kit (DICA-500, Bioassay Systems). Briefly, 5 µl of clarified supernatants was added to a 96-well plate, mixed with 100 µl QuantiChrom™ working solution, and incubated at room temperature for at least 3 minutes. In the presence of calcium, the QuantiChrom™ dye forms a blue-colored complex that absorbs maximally at 612 nm. The calcium concentrations are directly proportional to the intensity of the blue color and were calculated when fitted to a 12-point calibration curve with calcium chloride standards ranging from 0 mM to 4 mM.

Sample Preparation for ICP-MS

Selected samples from the 7-day time course were diluted with distilled water, filtered through a 0.2 µm PES syringe filter, and submitted for ICP-MS analysis to Actlabs (Ancaster, Ontario, Canada). A sample of the basalt powder used in these assays was analyzed by ICP-OES following Peroxide "Total" Fusion digestion.

Assessing sporulation.

To assess the presence of spores and to determine the sporulation efficiency of our strains during *in vitro* weathering assays and spent media experiments, 50 µl of homogenized cultures were mixed with 450 µl 1X PBS. The samples were serially diluted and plated onto LB agar to obtain total cell counts. In parallel, the diluted, homogenized cultures were incubated at 80 °C for 20 minutes to remove any heat-labile vegetative cells and to purify spores. The heat-treated samples were allowed to cool, serially diluted, then plated onto LB agar to obtain total spore counts.

Preparation of spent media.

Difco Nutrient Broth supplemented with 0.5% glucose was prepared with or without acid-washed basalt and incubated alone (UTC) or with Δ*spoIIE* for 3 days to allow for mineral dissolution. The samples were pelleted, and the supernatants were filter-sterilized to generate spent nutrient broth prepared without basalt ("-BA Spent NB"), or spent nutrient broth prepared with basalt ("+BA Spent NB"). MP2 and Δ*spoIIE* were then inoculated into either fresh nutrient broth (NB), -BA Spent NB, or +BA Spent NB, each in three independent biological replicates, then incubated at 30 °C for 3 days.

One-month basalt weathering assay.

Basalt (Ward's Scientific) disks were cut to 1.5 cm diameter and 0.3 cm thickness, polished using 400 grit silicon carbide, sonicated to remove particulates, then sterilized by autoclaving. The basalt disks were dried overnight at 60 °C before use. To visually observe weathering by our *B. subtilis* strains MP1, MP2, and Δ*spoIIE*, exponential phase cultures were diluted into nutrient broth supplemented with 0.5% glucose to a final OD_{600} of 0.1. Thirty milliliters of the cultures were transferred to 50 ml-beakers containing a sterilized basalt disk. The beakers were sealed with breathable membranes and incubated at room temperature, with minimal agitation (80 rpm).

After 30-days, the culture supernatants were decanted and stored at room temperature for soluble calcium measurements and spore and total cell enumeration (Supplemental Table S5). The basalt disks were gently rinsed three times with distilled H_2O. The basalt disks were dried overnight at 60 °C, carbon coated to a thickness of 15 nm, then imaged using a JEOL JSM IT800HL Scanning Electron Microscope (SEM). The SEM was equipped with a backscatter electron detector (BED) and a secondary electron detector (SED), and routinely operated at 10-20 kV.

REFERENCES

1. Walker, J. C. G., Hays, P. B. & Kasting, J. F. A negative feedback mechanism for the long-term stabilization of Earth's surface temperature. *J. Geophys. Res. Oceans* **86**, 9776–9782 (1981).
2. Brantley, S. L., Shaughnessy, A., Lebedeva, M. I. & Balashov, V. N. How temperature-dependent silicate weathering acts as Earth's geological thermostat. *Science (1979).* **379**, 382–389 (2023).
3. Trapp-Müller, G. *et al.* Earth's silicate weathering continuum. *Nat. Geosci.* **18**, 691–701 (2025).
4. Hartmann, J. *et al.* Enhanced chemical weathering as a geoengineering strategy to reduce atmospheric carbon dioxide, supply nutrients, and mitigate ocean acidification. *Reviews of Geophysics* **51**, 113–149 (2013).

5. Goll, D. S. *et al.* Potential CO2 removal from enhanced weathering by ecosystem responses to powdered rock. *Nat. Geosci.* **14**, 545–549 (2021).
6. Middelburg, J. J., Soetaert, K. & Hagens, M. Ocean Alkalinity, Buffering and Biogeochemical Processes. *Reviews of Geophysics* **58**, (2020).
7. Monger, H. C. *et al.* Sequestration of inorganic carbon in soil and groundwater. *Geology* **43**, 375–378 (2015).
8. Hasemer, H., Borevitz, J. & Buss, W. Measuring enhanced weathering: inorganic carbon-based approaches may be required to complement cation-based approaches. *Frontiers in Climate* **6**, (2024).
9. Kantola, I. B. *et al.* Improved net carbon budgets in the <scp>US</scp> Midwest through direct measured impacts of enhanced weathering. *Glob. Chang. Biol.* **29**, 7012–7028 (2023).
10. Holzer, I. O., Nocco, M. A. & Houlton, B. Z. Direct evidence for atmospheric carbon dioxide removal via enhanced weathering in cropland soil. *Environ. Res. Commun.* **5**, 101004 (2023).
11. Larkin, C. S. *et al.* Quantification of CO2 removal in a large-scale enhanced weathering field trial on an oil palm plantation in Sabah, Malaysia. *Frontiers in Climate* **4**, (2022).
12. Dietzen, C., Harrison, R. & Michelsen-Correa, S. Effectiveness of enhanced mineral weathering as a carbon sequestration tool and alternative to agricultural lime: An incubation experiment. *International Journal of Greenhouse Gas Control* **74**, 251–258 (2018).
13. Brooks, K. Rocks explained 2: Basalt. *Geology Today* **38**, 236–242 (2022).
14. Lewis, A. L. *et al.* Effects of mineralogy, chemistry and physical properties of basalts on carbon capture potential and plant-nutrient element release via enhanced weathering. *Applied Geochemistry* **132**, 105023 (2021).
15. Wilson, M. J. Weathering of the primary rock-forming minerals: processes, products and rates. *Clay Miner.* **39**, 233–266 (2004).
16. Sanderman, J. Can management induced changes in the carbonate system drive soil carbon sequestration? A review with particular focus on Australia. *Agric. Ecosyst. Environ.* **155**, 70–77 (2012).
17. Timmermann, T. *et al.* Harnessing Microbes to Weather Native Silicates in Agricultural Soils for Scalable Carbon Dioxide Removal. *Glob. Chang. Biol.* **31**, (2025).
18. Yang, Y. *et al.* Synergistic Effects of a Microbial Amendment and Crushed Basalt: Soil Geochemical and Microbial Responses. *Glob. Chang. Biol.* **32**, (2026).
19. Uroz, S., Calvaruso, C., Turpault, M.-P. & Frey-Klett, P. Mineral weathering by bacteria: ecology, actors and mechanisms. *Trends Microbiol.* **17**, 378–387 (2009).
20. Wild, B., Gerrits, R. & Bonneville, S. The contribution of living organisms to rock weathering in the critical zone. *Npj Mater. Degrad.* **6**, 98 (2022).
21. Finlay, R. D. *et al.* Reviews and syntheses: Biological weathering and its consequences at different spatial levels – from nanoscale to global scale. *Biogeosciences* **17**, 1507–1533 (2020).
22. Vicca, S. *et al.* Is the climate change mitigation effect of enhanced silicate weathering governed by biological processes? *Glob. Chang. Biol.* **28**, 711–726 (2022).
23. Mo, B. & Lian, B. Interactions between Bacillus mucilaginosus and silicate minerals (weathered adamellite and feldspar): Weathering rate, products, and reaction mechanisms. *Chinese Journal of Geochemistry* **30**, 187–192 (2011).

24. Ahmed, E. & Holmström, S. J. M. Siderophores in environmental research: roles and applications. *Microb. Biotechnol.* **7**, 196–208 (2014).
25. Basak, B. B. & Biswas, D. R. Influence of potassium solubilizing microorganism (Bacillus mucilaginosus) and waste mica on potassium uptake dynamics by sudan grass (Sorghum vulgare Pers.) grown under two Alfisols. *Plant Soil* **317**, 235–255 (2009).
26. Ribeiro, I. D. A. *et al.* Use of Mineral Weathering Bacteria to Enhance Nutrient Availability in Crops: A Review. *Front. Plant Sci.* **11**, (2020).
27. Štyriaková, I., Štyriak, I. & Oberhänsli, H. Rock weathering by indigenous heterotrophic bacteria of Bacillus spp. at different temperature: a laboratory experiment. *Mineral. Petrol.* **105**, 135–144 (2012).
28. Sheng, X. F. Growth promotion and increased potassium uptake of cotton and rape by a potassium releasing strain of Bacillus edaphicus. *Soil Biol. Biochem.* **37**, 1918–1922 (2005).
29. Han, X. *et al.* Phyllospheric application of Bacillus mucilaginosus mediates the recovery of tea plants exposed to low-temperature stress by alteration of leaf endophytic community and plant physiology. *BMC Microbiol.* **25**, 177 (2025).
30. Granger, A. C., Gaidamakova, E. K., Matrosova, V. Y., Daly, M. J. & Setlow, P. Effects of Mn and Fe Levels on Bacillus subtilis Spore Resistance and Effects of Mn2+, Other Divalent Cations, Orthophosphate, and Dipicolinic Acid on Protein Resistance to Ionizing Radiation. *Appl. Environ. Microbiol.* **77**, 32–40 (2011).
31. Paidhungat, M., Setlow, B., Driks, A. & Setlow, P. Characterization of Spores of Bacillus subtilis Which Lack Dipicolinic Acid. *J. Bacteriol.* **182**, 5505–5512 (2000).
32. Nishikawa, M. & Kobayashi, K. Calcium Prevents Biofilm Dispersion in Bacillus subtilis. *J. Bacteriol.* **203**, (2021).
33. Sinnelä, M. T., Pawluk, A. M., Jin, Y. H., Kim, D. & Mah, J.-H. Effect of Calcium and Manganese Supplementation on Heat Resistance of Spores of Bacillus Species Associated With Food Poisoning, Spoilage, and Fermentation. *Front. Microbiol.* **12**, (2021).
34. Weinberg, E. D. Manganese Requirement for Sporulation and Other Secondary Biosynthetic Processes of Bacillus. *Appl. Microbiol.* **12**, 436–441 (1964).
35. Eisenstadt, E., Fisher, S., Der, C.-L. & Silver, S. *Manganese Transport in Bacillus Subtilis W23 During Growth and Sporulation*. *JOURNAL OF BACTERIOLOGY* vol. 113 https://journals.asm.org/journal/jb (1973).
36. Hirota, R., Hata, Y., Ikeda, T., Ishida, T. & Kuroda, A. The silicon layer supports acid resistance of Bacillus cereus spores. *J. Bacteriol.* **192**, 111–116 (2010).
37. Li, L. *et al.* Optimization of sporulation and purification methods for sporicidal efficacy assessment on Bacillus spores. *J. Ind. Microbiol. Biotechnol.* **49**, (2022).
38. Scribner, H., Eisenstadt,' And, E. & Silver, S. *Magnesium Transport in Bacillus Subtilis W23 During Growth and Sporulation*. *American Societv for Microbiology* vol. 117 https://journals.asm.org/journal/jb (1974).
39. Song, W., Ogawa, N., Oguchi, C. T., Hatta, T. & Matsukura, Y. Effect of Bacillus subtilis on granite weathering: A laboratory experiment. *Catena (Amst).* **70**, 275–281 (2007).
40. Song, W., Ogawa, N., Takashima-Oguchi, C., Hatta, T. & Matsukura, Y. Laboratory experiments on bacterial weathering of granite and its constituent minerals. *Géomorphologie : relief, processus, environnement* **16**, 327–336 (2010).
41. Lybrand, R. A. *et al.* A coupled microscopy approach to assess the nano-landscape of weathering. *Sci. Rep.* **9**, 5377 (2019).

42. Radoslovich, E. W. Feldspar Minerals. in *Soil Components* 433–448 (Springer Berlin Heidelberg, Berlin, Heidelberg, 1975). doi:10.1007/978-3-642-65917-1_12.
43. Brady, P. V. & Walther, J. V. Controls on silicate dissolution rates in neutral and basic pH solutions at 25°C. *Geochim. Cosmochim. Acta* **53**, 2823–2830 (1989).
44. White, A. F. & Brantley, S. L. The effect of time on the weathering of silicate minerals: why do weathering rates differ in the laboratory and field? *Chem. Geol.* **202**, 479–506 (2003).
45. Daux, V., Guy, C., Advocat, T., Crovisier ', J.-L. & Stille ', P. *Kinetic Aspects of Basaltic Glass Dissolution at 90°C: Role of Aqueous Silicon and Aluminium*. *Chemical Geology* vol. 142 (1997).
46. Sriwastava, P., Saini, V. K., Mathew, G. & Shukla, A. D. Experimental pathways of clay formation and kinetics of basalt alteration in poor drainage systems: Implications for weathering. *Geochim. Cosmochim. Acta* **396**, 13–27 (2025).
47. Techer, I., Advocat, T., Lancelot, J. & Liotard, J.-M. *Dissolution Kinetics of Basaltic Glasses: Control by Solution Chemistry and Protective Effect of the Alteration Film*. *Chemical Geology* vol. 176 www.elsevier.comrlocaterchemgeo (2001).
48. Cunningham, C. J. *et al.* Carbon dioxide removal during dissolution of granular basalt: A mass balance test of enhanced rock weathering at the hillslope scale. *Earth Planet. Sci. Lett.* **671**, 119662 (2025).
49. Cole, T. L., Torres, M. A. & Kemeny, P. C. The Hydrochemical Signature of Incongruent Weathering in Iceland. *J. Geophys. Res. Earth Surf.* **127**, (2022).
50. Lee, M. R., Hodson, M. E. & Parsons, I. The role of intragranular microtextures and microstructures in chemical and mechanical weathering: direct comparisons of experimentally and naturally weathered alkali feldspars. *Geochim. Cosmochim. Acta* **62**, 2771–2788 (1998).
51. Parsons, I., Fitz Gerald, J. D. & Lee, M. R. Routine characterization and interpretation of complex alkali feldspar intergrowths. *American Mineralogist* **100**, 1277–1303 (2015).
52. Schwengers, O. *et al.* Bakta: rapid and standardized annotation of bacterial genomes via alignment-free sequence identification. *Microb. Genom.* **7**, (2021).
53. Hoover, S. E., Xu, W., Xiao, W. & Burkholder, W. F. Changes in DnaA-Dependent Gene Expression Contribute to the Transcriptional and Developmental Response of *Bacillus subtilis* to Manganese Limitation in Luria-Bertani Medium. *J. Bacteriol.* **192**, 3915–3924 (2010).

ACKNOWLEDGMENTS

We thank John L. Grimsich at the University of California, Berkeley's Earth and Planetary Science Department (EPS) for their help preparing and processing the basalt disks, and for their expertise and technical support on the JEOL JSM IT800HL Scanning Electron Microscope. We also thank Marjorie Schulz for their advice interpreting SEM images.

AUTHOR CONTRIBUTIONS

CY designed, planned, and managed the experiments. CY, KS, and AK performed the experiments and collected samples and data. TT, CY, PDW performed statistical analyses. CY, PDW, and TT wrote the first draft of the manuscript. CRL performed CrunchFlow and modeling experiments. GAFM and TT acquired funding for this study. All authors read, edited, and approved the final manuscript.

DATA AVAILABILITY

The datasets generated and/or analyzed during the current study are available from the corresponding author upon reasonable request.

FUNDING DECLARATION

This study was fully funded by Andes Ag, Inc.

CONFLICTS OF INTEREST

The authors declare potential competing interests as follows: Christopher Yip, Kira Stonkevitch, Abigail Knecht, Philip D. Weyman, Tania Timmermann, Corey R. Lawrence, and Gonzalo A. Fuenzalida-Meriz are employed by Andes Ag Inc., the company that funded this study.

FIGURES

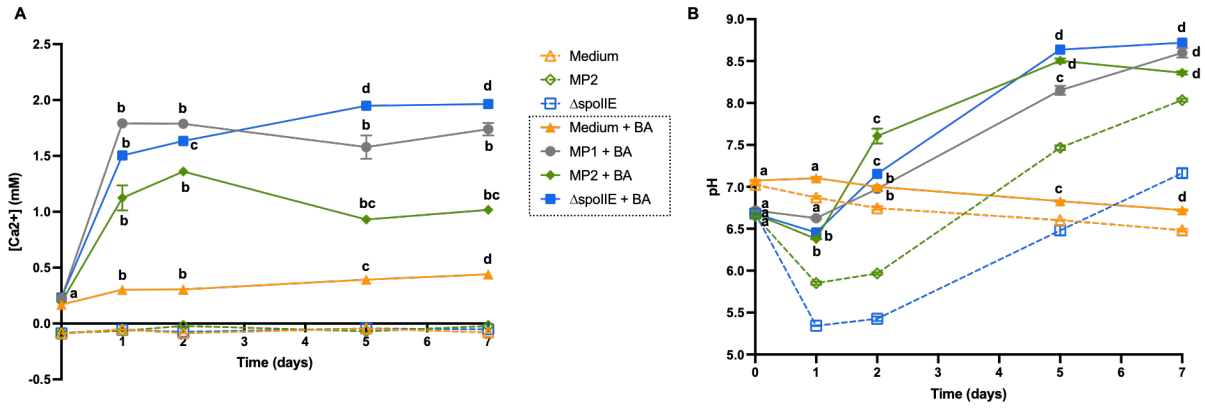

Figure 1. (A) Calcium release during *in vitro* weathering of basalt by *Bacillus subtilis* strains. MP1 (gray circles), MP2 (green diamonds), and a Δ*spoIIE* mutant (blue squares) were cultured in mB4-1 medium with or without basalt (BA) for seven days. Soluble calcium concentrations were quantified at the indicated time points. Data represent the mean +/- SE from biological replicates (n=3). One-way ANOVA and Tukey's multiple comparisons test were performed within each basalt treatment to determine significant differences among time points. Letters (a, b, c, or d) above each time point indicate statistically significant differences ($p < 0.05$). **(B) pH dynamics during *in vitro* weathering of basalt by *Bacillus subtilis* strains.** The pH of the cultures were measured at the indicated time points. Data represent the mean +/- SE from biological replicate (n=3). One-way ANOVA and Tukey's multiple comparisons test were performed within each basalt treatment to determine significant differences among time points. Letters (a, b, c, or d) above each time point indicate statistically significant differences ($p < 0.05$).

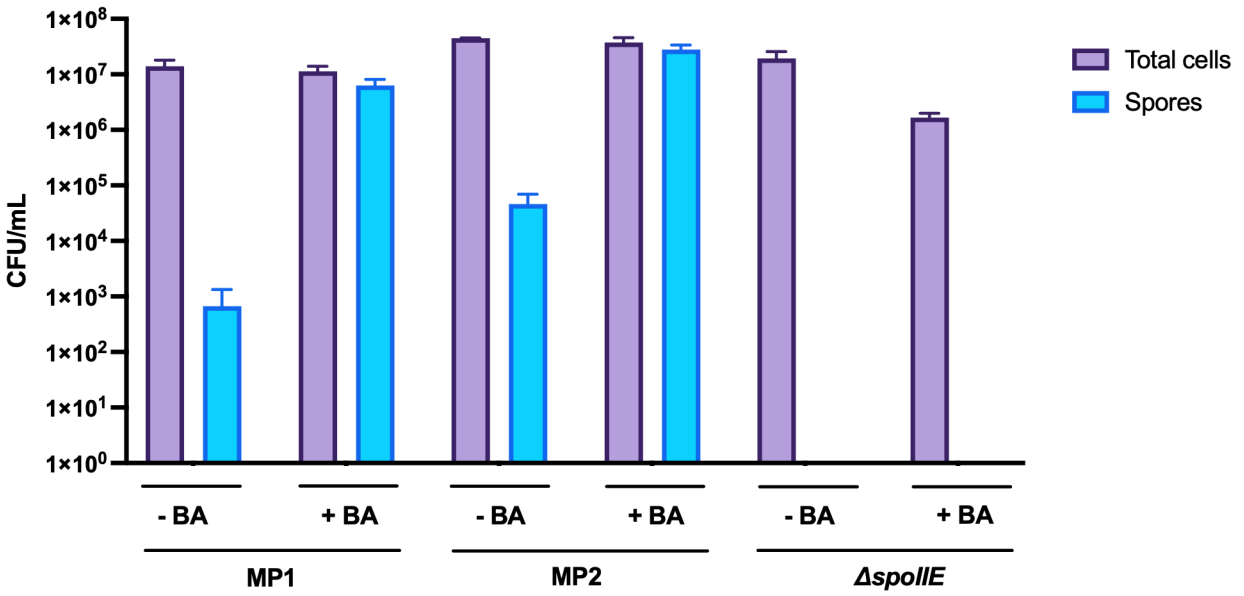

755

756 **Figure 2. *Bacillus subtilis* strains MP1 and MP2 sporulate under *in vitro* weathering**
757 **conditions.** Total viable cells (purple bars) and spores (blue bars) were enumerated from 3-day
758 cultures grown in mB4-1 medium in the presence (+BA) or absence of basalt (-BA). Data represent
759 the mean +/- SE from biological replicates (n=3).

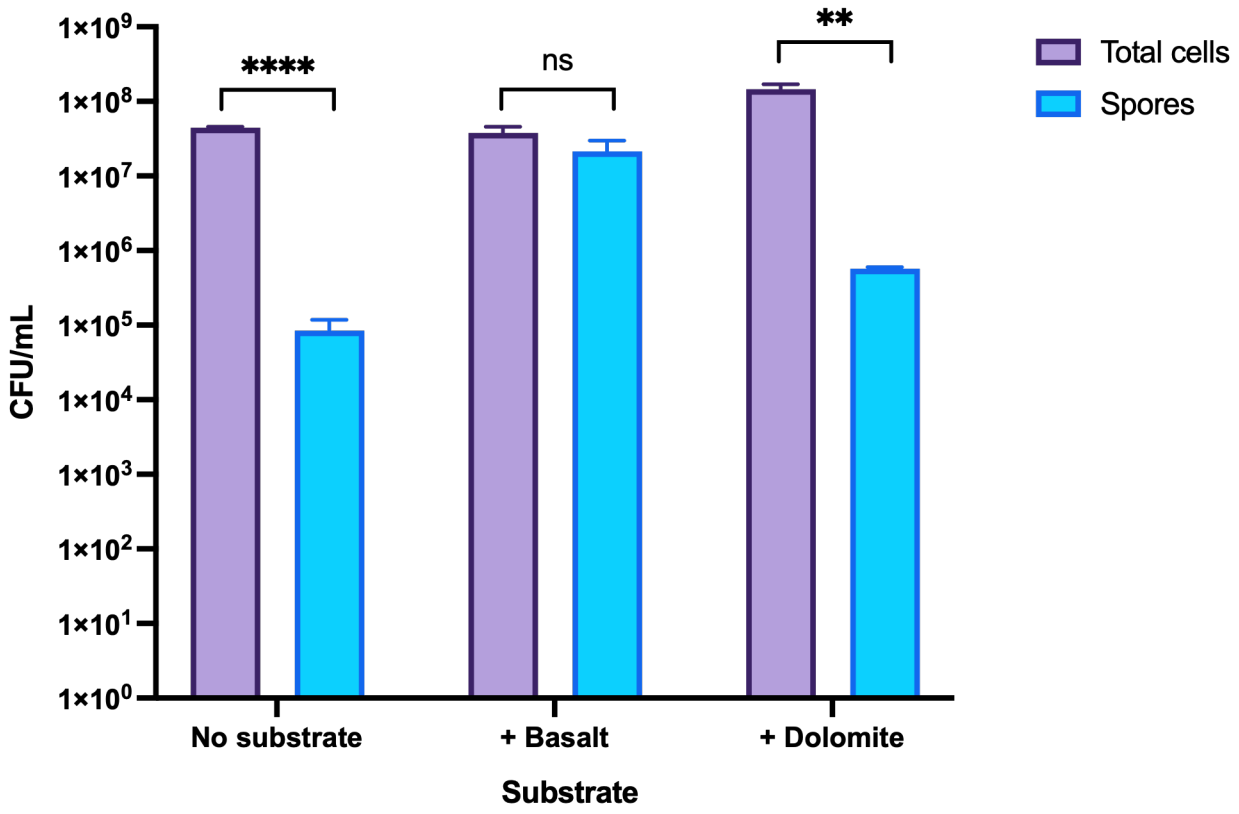

760

761 **Figure 3. Sporulation of *Bacillus subtilis* MP2 in the presence of mineral substrates.** Total
762 viable cells (purple bars) and spores (blue bars) were enumerated from 3-day MP2 cultures grown
763 in mB4-1 medium with or without basalt or dolomite. Data represent the mean +/- SE from
764 biological replicates (n=3). Asterisks above each bar indicate statistically significant differences
765 (unpaired t-test, ns: not significant, ** $p < 0.01$, **** $p < 0.0001$).

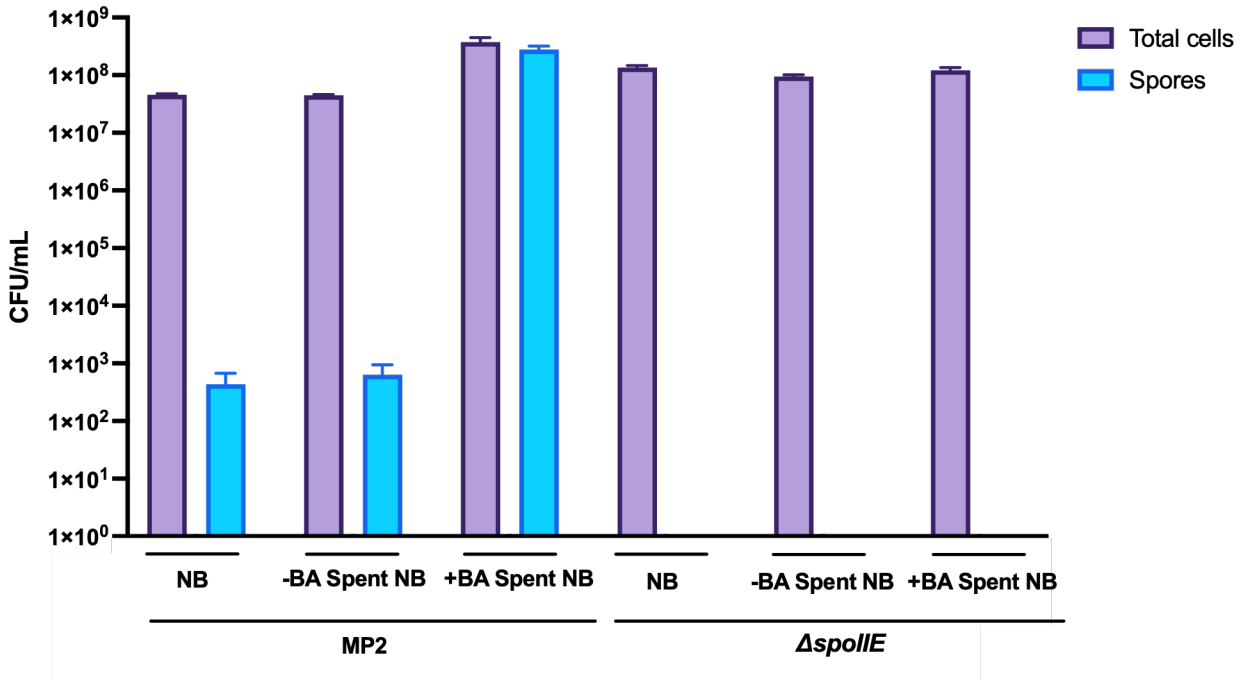

766

767 **Figure 4. Soluble products from basalt incubated with Δ*spoIIE* can induce MP2 sporulation.**

768 Δ*spoIIE* was grown in nutrient broth in the presence (+BA) or absence (-BA) of basalt for 3 days,

769 then the culture supernatants were filter-sterilized to generate spent media (Spent NB).

770 Subsequently, MP2 and Δ*spoIIE* were cultured in fresh nutrient broth (NB), spent NB lacking

771 basalt (-BA Spent NB), and spent NB with basalt (+BA Spent NB). The purple bars represent total

772 cell CFU/ml and the blue bars represent total spore CFU/ml. Δ*spoIIE* produced no spores in any

773 of the conditions tested. Data represents the mean +/- SE from biological replicates (n=3).

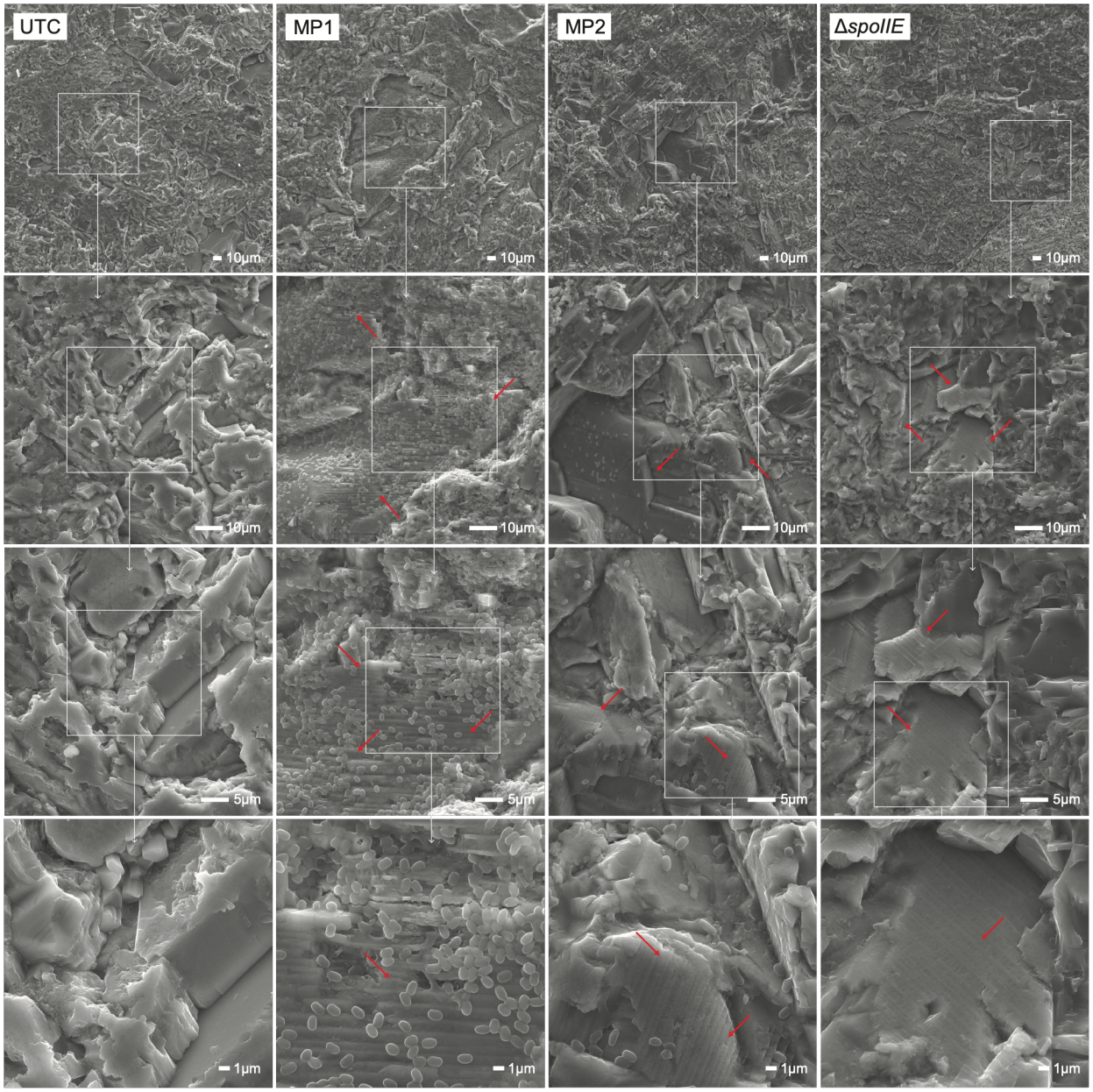

774

775 **Figure 5. Scanning electron micrographs of basalt surfaces following 30-day incubation with**
776 ***B. subtilis* strains.** Uninoculated basalt disks (UTC) displayed smooth crystalline planes with no
777 visible evidence of microbial colonization. In contrast, basalt surfaces incubated with MP1 and
778 MP2 were densely populated with numerous ovoid spores, visible along striations/crystalline
779 planes (red arrows). The striations closely resemble feldspar twinning, a phenomenon related to
780 geometric crystal growth. Images were acquired at 300x (top row), 1000x (second row), 2000x

781 (third row), and 4000x (bottom row) magnification. Scale bars = 10 μm (top panel) and 1 μm
782 (bottom panel).

Supplementary Information for "*Bacillus subtilis*-mediated weathering of basalt revealed through sporulation"

Christopher Yip[1], Kira Stonkevitch[1,#], Abigail Knecht[1,#], Philip D. Weyman[1], Tania Timmermann[1], Corey R. Lawrence, Gonzalo A. Fuenzalida-Meriz[1,]*

[1] Andes Ag, Inc., Alameda, CA, USA

[*] Corresponding author: Gonzalo A. Fuenzalida-Meriz, gonzalofuenzalida@gmail.com

[#] KS and AK contributed equally to this manuscript

FIGURES AND TABLES

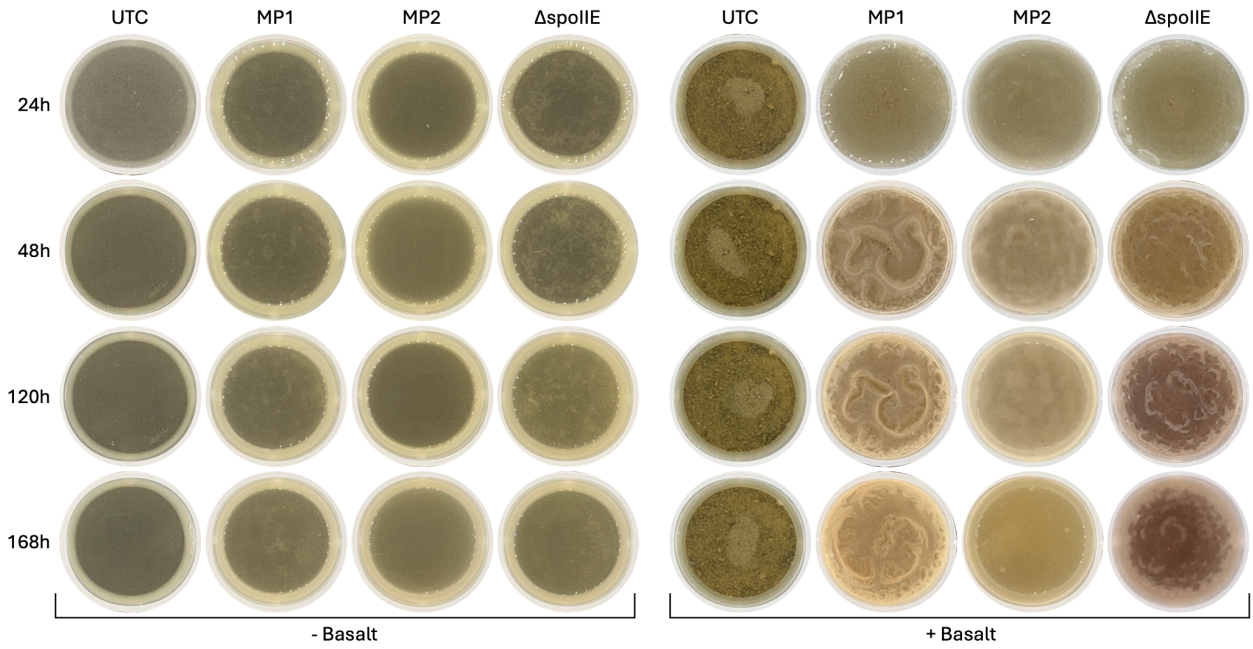

Supplemental Figure S1. *Bacillus subtilis* MP1, MP2, and Δ*spoIIE* growth phenotypes in the presence and absence of basalt. Images of the weathering plates were captured from above at the indicated timepoints. *Bacillus subtilis* MP1, MP2, and Δ*spoIIE* were cultured in mB4-1 in the presence and absence of 50 mg basalt. In the presence of basalt, robust pellicle biofilms were observed after 48-hours.

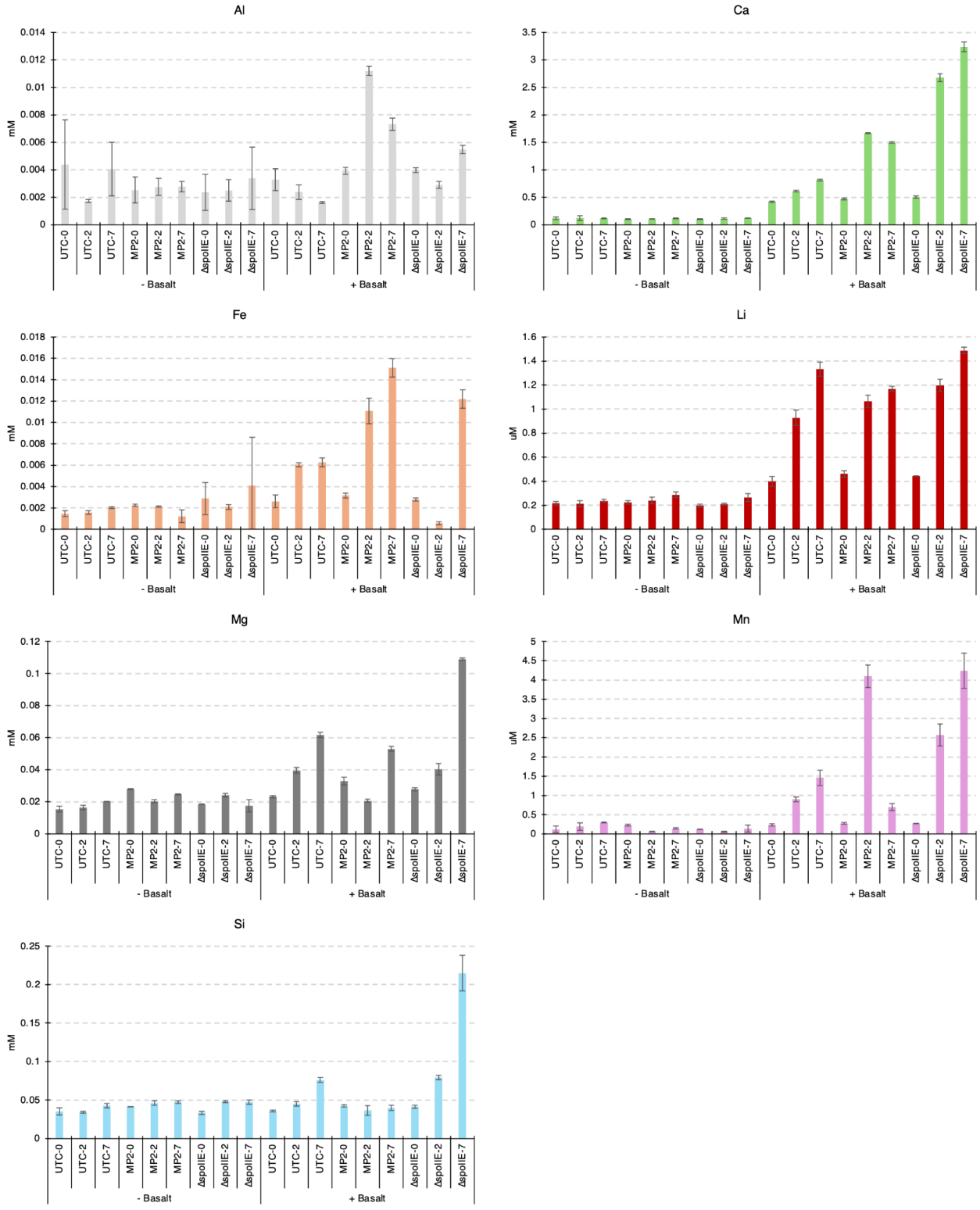

Supplemental Figure S2. ICP-MS analysis of culture supernatants. ICP-MS analysis of aluminum (Al), calcium (Ca), iron (Fe), lithium (Li), magnesium (Mg), manganese (Mn), and

silicon (Si) from selected sample supernatants from the 7-day time course experiment (Figure 1; days 0, 2, and 7). Data represent the mean +/- SD from independent samples (n=3).

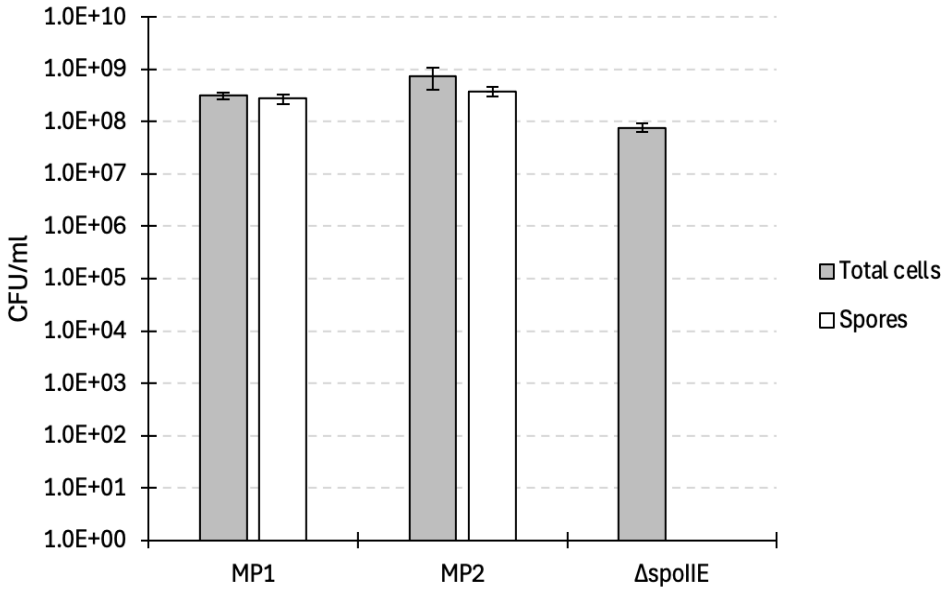

Supplemental Figure S3. *Bacillus subtilis* strain Δ*spoIIE* is impaired in its ability to sporulate while the wild-type strains MP1 and MP2 are not. Total cells and heat-resistant spore counts after 2 days of incubation in a media that promotes sporulation (DSM). Data represent the mean +/- SD from biological replicates (n=3).

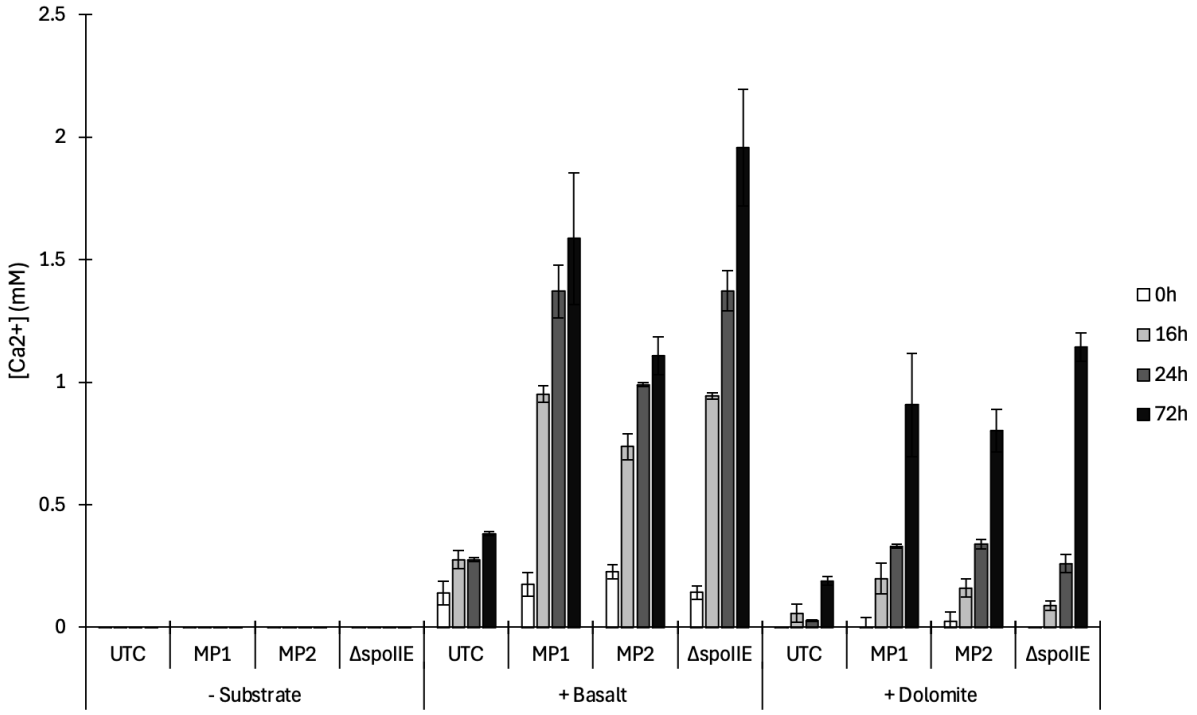

Supplemental Figure S4. Calcium release during *in* vitro weathering of basalt and dolomite by *Bacillus subtilis* strains MP1, MP2, and Δ*spoIIE*. MP1, MP2, and Δ*spoIIE* were cultured in mB4-1 medium with or without basalt and dolomite for three days. Soluble calcium concentrations were quantified at indicated timepoints. MP1, MP2, and Δ*spoIIE* released higher levels of calcium in the presence of both basalt and dolomite. Data represent the mean +/- SD from biological replicates (n=3).

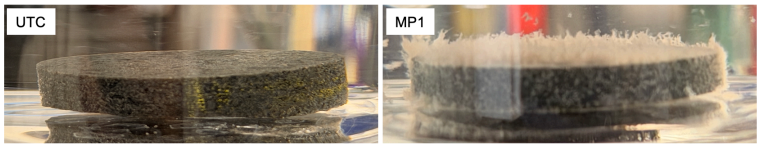

Supplemental Figure S5. Basalt disks after 30-day incubation. Basalt disks resuspended in distilled H_2O demonstrate dense colonization by MP1, a necessary condition for weathering, as evidenced by the thick biofilm associated with the silicate rock. Biomass and exopolysaccharides associated with biofilms are visually absent from the UTC sample.

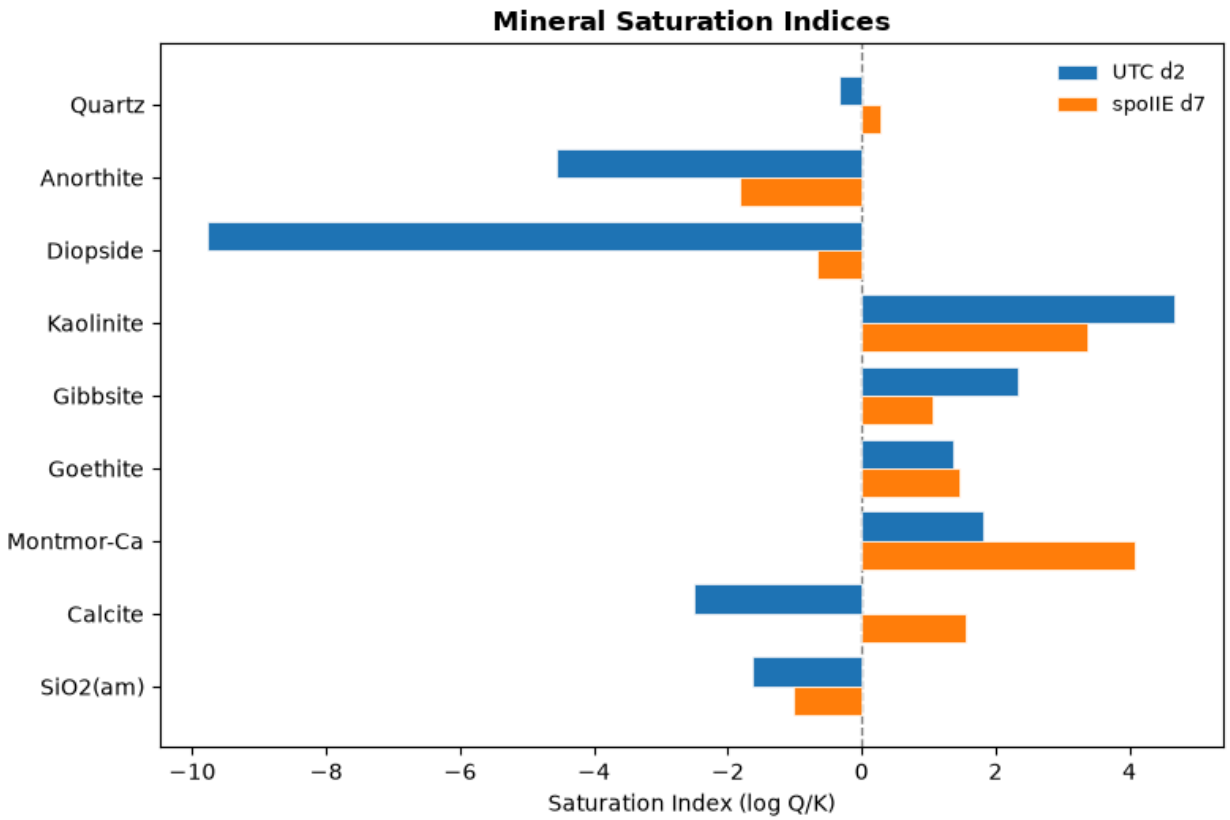

Supplemental Figure S6. Estimated secondary mineral saturation indices. Predicted secondary mineral saturation indices using CrunchFlow (speciate-only) based on the highest measured calcium release (day 2 for UTC and day 7 for ΔspoIIE) and corresponding measured pH values.

Mineral	Basalt (%)
Quartz	4
Oxides	4
Pyroxene/Amphibole	50
Feldspars	42

Table S1. The mineral abundance of BrixBlend basalt was estimated via a combination of semi-quantitative XRD and SEM-EDS.

Oxide	Basalt (%)
SiO_2	49.1
TiO_2	0.9
Al_2O_3	13.0
FeO*	15.9
MnO	0.2
MgO	6.6
CaO	10.1
Na_2O	2.8
K_2O	0.5
P_2O_5	0.0
LOI %	3.1

Table S2. Elemental abundance of major oxides in BrixBlend basalt measured by XRF. Loss-on-ignition (LOI) represents the mass of volatile compounds in the sample, including organic matter and structural water in clays. *Indicates total iron calculated as FeO.

Element	Basalt (%)	Element	Basalt (%)
Si	24.4	Pb	0.00044
Fe	10.2	Nb	0.00036
Al	6.99	Gd	0.00035
Ca	6.7	Er	0.00032
Mg	3.52	Yb	0.00031
K	0.6	Sm	0.00029
Ti	0.53	Pr	0.00023
Mn	0.162	Th	0.00019
P	0.05	Ge	0.00013
V	0.0334	Ho	0.00011
S	0.03	Eu	0.0001
B	0.017	U	0.00009
Sr	0.0158	Cs	0.00007
Ba	0.0122	Sn	0.00007
Zn	0.011	Tb	0.00007
Cu	0.0058	W	0.00007
Co	0.00456	Tm	0.00005
Cr	0.004	Tl	0.00001
Ni	0.004	Hf	<0.001
Li	0.00279	Se	<0.0008
Y	0.00274	Te	<0.0006
Rb	0.00197	Be	<0.0003
Ga	0.00184	Bi	<0.0002
As	0.0018	Cd	<0.0002
Ce	0.00167	Sb	<0.0002
Nd	0.00106	Mo	<0.0001
La	0.00087	In	<0.00002
Dy	0.00045	Ta	<0.00002

Table S3. Elemental analysis of BrixBlend basalt measured by ICP-OES following Peroxide "Total" Fusion metal recovery methodology.

Sample		UTC	MP2	Δ*spoIIE*
Nutrient Broth (NB)	Viable cells (CFU/ml)	0.00E+00	4.57E+07	1.35E+08
	Viable spores (CFU/ml)	0.00E+00	4.33E+02	0.00E+00
Sporulation Frequency (%)		**0**	**0.00**	**0**
ΔspoIIE Spent NB, -BA	Viable cells (CFU/ml)	0.00E+00	4.50E+07	9.47E+07
	Viable spores (CFU/ml)	0.00E+00	6.33E+02	0.00E+00
Sporulation Frequency (%)		**0**	**0.00**	**0**
UTC Spent NB, -BA	Viable cells (CFU/ml)	0.00E+00	1.71E+08	5.33E+08
	Viable spores (CFU/ml)	0.00E+00	4.80E+07	0.00E+00
Sporulation Frequency (%)		**0**	**28.13**	**0**
ΔspoIIE Spent NB, +BA	Viable cells (CFU/ml)	0.00E+00	3.73E+08	1.22E+08
	Viable spores (CFU/ml)	0.00E+00	2.77E+08	0.00E+00
Sporulation Frequency (%)		**0**	**74.11**	**0**

Table S4. Total viable CFUs, spore CFUs, sporulation frequencies from spent media experiments.

Sample	Total Viable Cells (CFU/ml)	Total Spores (CFU/ml)	Sporulation Frequency (%)	Soluble Ca improvement over UTC (%)
UTC	0.00E+00	0.0E+00	0.0	
MP1	6.02E+07	5.1E+07	82.3	210.1
MP2	7.80E+07	3.7E+07	47.4	126.4
Δ*spoIIE*	6.91E+06	0.0E+00	0.0	109.7

Table S5. Total viable CFUs, spore CFUs, sporulation frequencies, and soluble calcium measurements from 30-day basalt weathering samples.